

Orbital (Two-Channel) Kondo Effect Problem in Nonmagnetic PbFCl-Type Pnictide Chalcogenides

Tomasz Cichorek¹, Rainer Niewa², Marcus Schmidt, Andreas Schlechte, Reiner Ramlau, Gudrun Auffermann, Yurii Prots, Adriana Sanchez, Philipp Gegenwart, Franziska Weickert, Silke Paschen³, Walter Schnelle, Andrzej Wojakowski⁴, Zygmunt Henkie⁴, Frank Steglich, and Rüdiger Kniep

Since the pioneering work by Nozières and Blandin [1], the search for a two-channel Kondo (2CK) effect has been the subject of considerable scientific interest. However, its experimental realization requires a strict channel symmetry that is hard to achieve in the spin (magnetic) Kondo problem. As a viable alternative, one may consider an equivalent (nonmagnetic) Kondo effect that originates from scattering centers with orbital degrees of freedom instead of spin ones like, e.g., the electric quadrupole momenta in certain heavy-fermion systems [2]. In this so-called orbital Kondo effect, the spin of the conduction electrons, playing the role of a silent channel index, is not directly involved in the scattering process. For this reason, the influence of a magnetic field on the orbital Kondo resonance is very weak and, therefore, distinctly different from the destruction of the spin Kondo resonance by a relatively low magnetic field. As originally suggested by Zawadowski [3], the interaction between structural two-level systems (TLS) and the conduction electrons may also lead to the orbital Kondo effect and the resultant 2CK problem. In this model, a single tunneling center (e.g., a particle that quantum-mechanically tunnels between two minima of a double-well potential) immersed in the Fermi sea is expected to behave like a spin-1/2 impurity coupled to the conduction electrons. However, it is still debatable whether the strong-coupling 2CK fixed point due to the TLS can actually be reached experimentally [4,5].

Physical properties of ThAsSe and UAsSe compounds

Our previous work on the diamagnetic system with the approximate composition ThAsSe (PbFCl-type structure, $P4/nmm$) has demonstrated the importance of tunneling states to the charge transport in a real metal [6,7]: At temperatures lower than about

20 K, a logarithmic increase of the electrical resistivity $\rho(T)$ upon cooling was found. This $-\log T$ anomaly, together with its independence on both strong magnetic fields and high hydrostatic pressures, point to a Kondo effect derived from structural TLS. According to X-ray and transmission-electron-microscopy studies, and remarkably similar transport properties of the ferromagnetic counterpart UAsSe, tunneling centers seem to be located in the structurally disordered As-Se sublattice [8].

Very recent examinations of the low-temperature thermal properties of single-crystalline ThAsSe directly revealed the presence of movable defects [9]. In fact, as depicted in Fig. 1, both the thermal conductivity $\kappa(T)$ and the specific heat $c_p(T)$ show features typical for matter with dynamical disorder. This holds especially true for a $T^{1.97}$ contribution to $\kappa(T)$ (in the absence of significant phonon-electron scattering) and a quasilinear-in- T term (of nonelectronic origin) in $c_p(T)$.

Electronic transport properties of the same single crystal of ThAsSe are shown in Fig. 2a. Below about 16 K, an additional contribution to $\rho(T)$ emerges. Here we plotted the relative change of the resistivity normalized to the corresponding value at 1 K, $\Delta\rho / \rho_{1K}$. For $T \leq 0.9$ K and $B = 0$, the resistivity levels off. If a magnetic field $B \geq 1$ T is applied then the resistivity depends strictly linearly on $T^{1/2}$ in a wide temperature window, i.e., from around 0.16 K to above 12 K at $B = 14$ T. The coefficient of the $-AT^{1/2}$ term amounts to $A = 0.38 \mu\Omega\text{cm}/\text{K}^{1/2}$ for all fields $B \geq 1$ T.

The field-independent increase $T^{1/2}$ of $\rho(T)$ observed upon lowering the temperature can neither be attributed to weak localization nor to electron-electron interactions in a three-dimensional disordered system. In fact, both types of quantum corrections to the resistivity are highly sensitive to magnetic fields. For example, the interference of the wave functions of the electrons moving along a closed loop is weakened or even destroyed by a

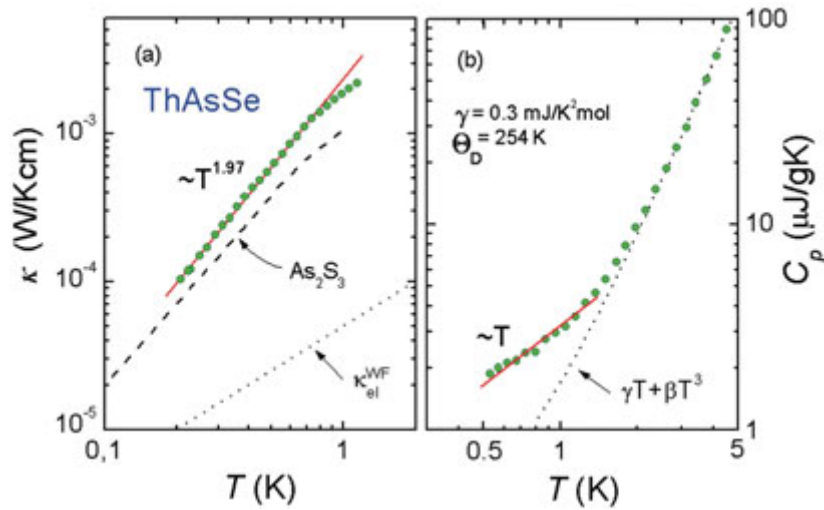


Fig. 1. Low-temperature thermal properties of a ThAsSe single crystal. (a): Total thermal conductivity (circles) and estimated electronic contribution, κ_{el}^{WF} (dotted line), as a function of temperature. The solid line is a fit with a $T^{1.97}$ power-law dependence. For comparison, $\kappa(T)$ of the dielectric glass is also shown. (b): Specific heat as a function of temperature in a double-logarithmic plot (circles). The dotted line shows the $\gamma T + \beta T^3$ dependence with $\beta = 3 \times 1944 / \Theta_D^3$ in units of $J/K^4 \text{mol}$, implying a Debye temperature of $\Theta_D = 254$ K and $\gamma = 0.3 \text{ mJ/K}^2 \text{mol}^{-1}$, the Sommerfeld coefficient of the electronic specific heat. The solid line indicates the presence of an additional (non-electronic) linear-in- T term due to TLS.

magnetic field of the order of tens of an Oersted only. We, therefore, attribute the field-independent $-AT^{1/2}$ term in the electrical resistivity to electron scattering off the TLS. This is, to our knowledge, the first-ever observation of the 2CK state originating from TLS in a macroscopic system.

A deviation of the zero-field resistivity from the $-AT^{1/2}$ behavior below 1 K followed by its disappearance in a magnetic field as small as 0.2 T is surprising in the context of nonmagnetic electron-TLS interaction. Therefore, we suppose that the 2CK effect in the weak field limit is hidden by another phenomenon being suppressed already at $B \approx 1$ T. To explore this possibility further, the isothermal response of the resistivity to a magnetic field was studied (Fig. 2b). The measurements were performed in the temperature window $0.1 \leq T \leq 10$ K where the $-AT^{1/2}$ dependence was observed in $\rho(T)$. A positive MR whose magnitude gradually decreases with increasing temperature is found at $B < 1$ T only. At 10 K, $(\rho_B - \rho_0)/\rho_0$ is practically zero within this field range. Most likely, this low-field positive magnetoresistivity reflects spin-orbit scattering that rotates the spin of the conduction electrons and yields a destructive interference of the electron wave functions. Consequently, the differences between the results obtained at $B \leq 0.2$ T and those obtained at $B \geq 1$ T, as depicted in Fig.

2(a), are tentatively ascribed to (spin-orbit-derived) quantum corrections.

Whereas a small and negative MR is characteristic for ThAsSe [9], an MR decreasing as $B^{1/2}$ has been observed only at $T \leq 10$ K. Additionally, the slope of this isothermal $B^{1/2}$ dependence (in units of $\mu\Omega\text{cm}/T^{1/2}$) amounts to 0.77 and is larger by a factor of ≈ 2 than that of the iso-field $T^{1/2}$ dependence ($= 38$ in units of $\mu\Omega\text{cm}/\text{K}^{1/2}$). Though not yet understood, this relationship between the negative MR and the occurrence of the extra $-AT^{1/2}$ term in $\rho(T)$ found for $T \leq 12$ K and $B \geq 1$ T is very intriguing. Both observations clearly point to a characteristic energy scale of a few K for the 2CK effect in ThAsSe. This is in striking contrast to most of the theoretical considerations which predict a Kondo temperature T_K of orders of magnitude lower than 1 K for the orbital Kondo problem due to the TLS. We believe that the nature of tunneling centers is a key parameter to understand this discrepancy. In fact, certain peculiarities of the crystal structure of ThAsSe like, e.g., a gradual formation of covalently bonded dimers $(\text{As}-\text{As})^{4-}$ [10], led us to speculate that the movable particle is an electron rather than an atom: T_K of a few K in ThAsSe would then be the consequence of the electron mass being smaller than the atomic masses by about four orders of magnitude.

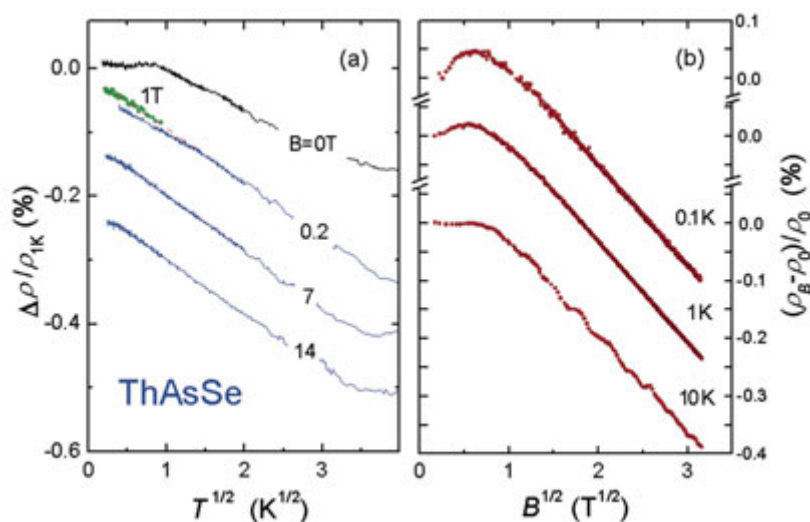


Fig. 2. (a) Low-temperature electrical resistivity of ThAsSe as $\Delta\rho / \rho_{1K}$ vs $T^{1/2}$ in varying magnetic fields applied along the c axis. For clarity, the different curves in $B > 0$ were shifted subsequently by 0.1 %. Circles display the $B = 1$ T data, and the red dashed line represents a $-AT^{1/2}$ behavior with $A = 0.38 \mu\Omega\text{cm}/\text{K}^{1/2}$, independent of magnetic field at $B \geq 1$ T. (b) Magnetic-field dependence of the resistivity of the same ThAsSe single crystal at low temperatures where a $-AT^{1/2}$ term is observed.

Zr-based compounds

In order to clarify the underlying mechanism, we have extended our studies to the isotype Zr-based arsenide selenides and tellurides [11,12]. These free-of-actinide systems have several advantages with respect to the counterpart ThAsSe: The handling is simplified due to the less poisonous metallic component. Additionally, crystals can be produced via chemical transport in higher purity since Zr shows less attack to fused silica used as ampoule material. The resulting products are favorable to study by X-ray and neutron diffraction techniques, due to the preferable form factor and preferable scattering length relations compared to the uranium and thorium systems. As a result, these advantages put us into a position to study the related systems Zr-As-Se and Zr-As-Te in deep detail, as will be described in the following.

Synthesis

Due to the thermo-chemical properties of ternary compounds of the system Zr/As/Se, which are characterized by high selenide and arsenide partial pressures below the melting temperatures, and to the concurrent possibility of forming volatile iodides of zirconium, the chemical transport should represent a preferred and suitable method for the crystalliza-

tion of the target compounds. In particular, for compounds which decompose during melting, show phase transformations, or high decomposition pressures at the melting point, chemical transport is an alternative for growing crystals from the melt. Chemical transport is characterized by the fact that solid or liquid material reacts with a gaseous transport agent in heterogeneous reactions creating gaseous species. Subsequent to the material transport a reformation takes place. The potential gradient as the driving force for material transport between the dissolution and the deposition sides is, as a rule, achieved by temperature differences. Starting from micro-crystalline powder samples, the arsenide selenide crystallized by an exothermal transport reaction in a temperature gradient from 1123 K (source) to 1223 K (sink). As a particular difficulty, chemical transport experiments are usually conducted in evacuated sealed silica tubes. The principal problem in this respect is the thermodynamic stability of zirconium dioxide which is significantly higher as compared with the tube material. The consequence is that zirconium dioxide and silicides are formed by redox reactions with the tube material, as well as silicates in subsequent reactions. By applying sealable glassy carbon tubes such undesired side-reactions with the tube material can be largely prevented.

After first thermodynamic considerations it is possible to approximately describe the exothermal

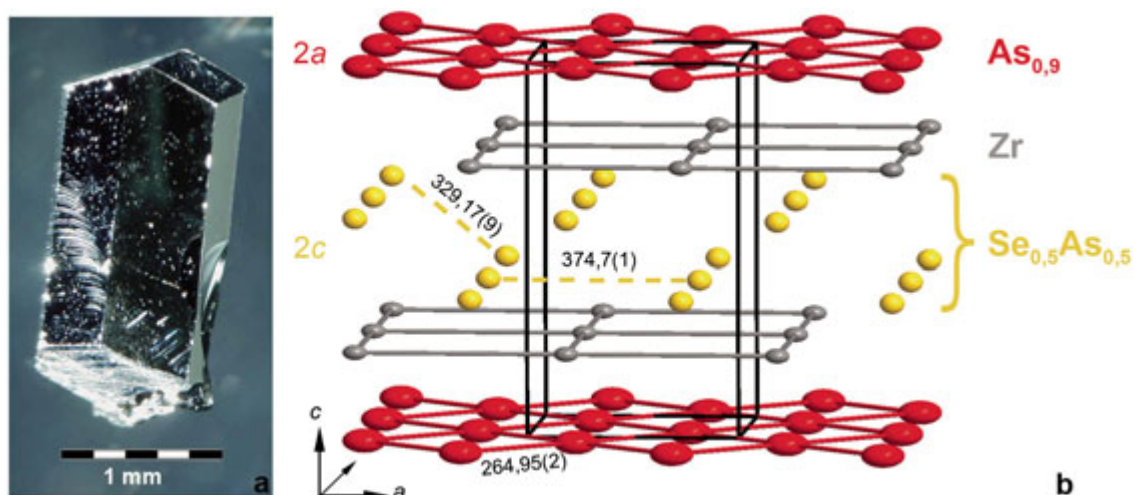
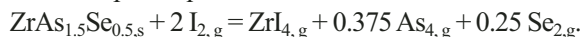


Fig. 3: a) Light microscopy image of a single crystal of $\text{ZrAs}_{1.4}\text{Se}_{0.5}$. b) Crystal structure of $\text{ZrAs}_{1.4}\text{Se}_{0.5}$ with the 2c site equally occupied by As and Se (yellow) and 10 % deficiency on the 2a site (red). As-As distances are given in pm. The larger displacement parameters of As on 2a perpendicular to [001] should be pointed out.

transport behavior observed by the following formal transport equilibrium



Characterization

The crystals obtained (Fig. 3a) were comprehensively characterized by electron-probe micro-analysis, wavelength-dispersive X-ray spectroscopy (WDXS), transmission electron microscopy, X-ray diffraction on single crystals and microcrystalline powder, gas pycnometry as well as by chemical analyses applying the ICP-OES (Inductively-Coupled-Plasma–Optical-Emission-Spectrometry) method. Part of one selected single crystal which forms the basis for all investigations carried out (except chemical analysis), was embedded plane-parallel to a well-formed prism face and processed metallographically. WDXS based on the respective element standards was applied for the quantitative analysis. Quantification was achieved by analyzing of the respective contributions of the characteristic X-radiation stemming from the individual elements. It could be shown that the investigated crystal was chemically homogeneous, did not contain any constituents of the transport agent, but did contain traces of silicon. The atomic ratio of elements and their standard deviations determined at ten measuring points on the single crystal were yielded for Zr: 34.69 ± 0.04 at.%, for As: 48.51 ± 0.05 at.% and for Se: 16.80 ± 0.02 at.%. This resulted in the

chemical composition of $\text{Zr}_{1.000(1)}\text{As}_{1.398(1)}\text{Se}_{0.484(1)}$.

Further investigations of the composition were carried out on several single crystals by means of the ICP-OES method. For this purpose, suitable digestion reagents and digestion conditions for the precise and simultaneous determination of zirconium, arsenic and selenium were at first ascertained in pre-investigations on micro-crystalline material with an ICP spectrometer. The single crystals (each between 2 and 10 mg) were digested in a mixture of HNO_3 conc. (2 ml) and $\text{HF}_{\text{conc.}}$ (20 μl per 5 mg of weighed-in quantity). The amount of HF needed to completely dissolve the samples was low enough for the measurements to be carried out with an equipment of a glass concentric nebulizer, a twister-cyclon glass spray chamber and a quartz torch with an alumina injector tube for obtaining higher measuring precision. Calibration was performed by matrix-matched Zr, As, Se standard solutions (0 – 50 mg/l each). Spectral interferences did not occur. The analytical results show that the arsenic and selenium contents in all five single crystals investigated are inversely correlated; however, they merely vary from sample to sample within a narrow range of concentration. The total formula established for the ternary compound is obtained when scaled with respect onto zirconium (1.0). Considering all five single crystals we obtained a composition $\text{Zr}_{1.000(7)}\text{As}_{1.38(1)}\text{Se}_{0.49(1)}$ which agrees well with the values established by means of the WDXS analysis performed on another crystal.

Crystal structure

The structure refinement by single crystal X-ray diffraction ($P4/nmm$, $a = 374.69(1)$ pm, $c = 807.16(1)$ pm) results in the total formula $ZrAs_{1.40}Se_{0.50}$ or $ZrAs_{0.90(1)}(Se_{0.50(1)}As_{0.50})$, respectively, thus well agreeing with the results of WDXS and ICP-OES. The total formula of the ternary compound seems to correlate also with its range of existence and should not be regarded as an accidental result of the substitution series. The ternary compound crystallizes in the UPS-type branch of the $PbFCl$ aristo-type, a substitution variant of the Fe_2As structure type, also called $ZrSiS$ structural type. In this case, the larger anions typically occupy a $2c$ site while the smaller anions occupy the $2a$ site. The anions may principally be distributed on both sites in the sense of substitution. In the case of $ZrAs_{0.90(1)}(Se_{0.50(1)}As_{0.50})$, the $2c$ site is equally occupied by selenium and arsenic, and there is a 10 % deficiency in As occupancy of the $2a$ site (Fig. 3b).

Closer inspection of the displacement parameters of arsenic reveals a larger lateral displacement as compared with the displacement in $[001]$. In agreement with the tendency of arsenic towards the formation of homo-atomic bonds, this can be inter-

preted as an indication of forming covalent As–As bonds along with the formation of polymeric units. Both, this situation and the almost 1:1 occupancy of $2c$ sites can lead to super-structures or local order in the real structure which might, however, hardly be detectable by X-ray diffraction methods. The comparison of density obtained from X-ray diffraction with that one established by gas pycnometry of 6.9661 g/cm³ or $6.965(5)$ g/cm³, respectively, shows no significant difference.

Real structure by electron microscopy

For the high-resolution transmission electron microscopy (HRTEM) and the electron diffraction at $T = 293$ K parts of the characterized single crystal were crushed further. Micro-crystallites of orientations $[001]$, $[100]$ and $[110]$ could successfully be investigated. In the HRTEM images, however, neither a possible order of the As atoms nor vacancies on the $2a$ site, nor order of the As and Se atoms on the $2c$ site, could be confirmed (Fig. 4a). Nonetheless, the electron diffraction diagrams in the $[001]$ orientation (Fig. 4b) refer to some order phenomenon. Apart from Bragg reflections, extremely weak, diffuse satellite reflections $\mathbf{G} \pm \mathbf{q}_1$

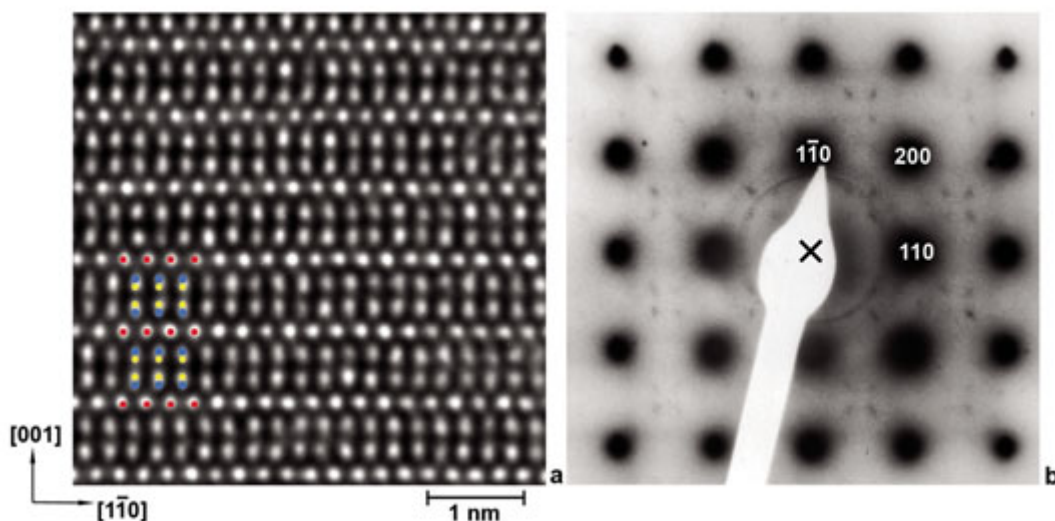


Fig. 4: Micro-crystallites of $ZrAs_{1.4}Se_{0.5}$ were investigated with the help of an electron microscope Tecnai F30-G2 (acceleration voltage: 300 kV, point resolution: 0.2 nm). a) HRTEM image in $[110]$ orientation. The Zr atoms cannot be separated from the As and Se atoms, respectively, on the $2c$ site since their distance in the projection amounts to merely 0.09 nm (cf. inserted structural image). Sample thickness: $t \approx 5$ nm; defocussing: $\Delta f \approx -75$ nm.

b) Selected-area electron diffraction pattern in $[001]$ orientation. Since a proof of the extremely weak satellite reflections by means of a CCD camera failed, a photographic negative had to be strongly super-exposed and reproduced appropriately. As a result, the intensity of the satellite reflections, as compared with the intensity of the Bragg reflections, is shown heavily exaggerated.

and $\mathbf{G} \pm \mathbf{q}_2$ can be recognized. They surround the forbidden reflections $\mathbf{G} = [hk0]^*$, $h + k$ odd, and are described by the modulation vectors $\mathbf{q}_1 = \gamma \cdot [100]^*$ and $\mathbf{q}_2 = \gamma \cdot [010]^*$, with $\gamma \approx 0.28$. Because of the diffuse character of the satellite reflections, γ cannot be exactly be determined; the modulation is, however, regarded as incommensurate. A very similar picture (with the same \mathbf{q}_1 , \mathbf{q}_2 and γ) was recently described for ThAsSe at temperatures between 30 K and 100 K [10] and put into the context of a two-dimensional long-range ordered As–As dimerization in the networks parallel to (001). In the case of $\text{ZrAs}_{1.40}\text{Se}_{0.50}$, ordering (bond formation) in both, the As layers (2a site) and the As–Se layers (2c site) is possible. Unfortunately, first attempts to amplify the very weak diffraction effects by applying an LN₂ cryogenic device were not successful. It is planned to prepare massive, pre-oriented specimens from the largest available $\text{ZrAs}_{1.40}\text{Se}_{0.50}$ single crystals and to intensify electron-microscopic investigations.

Physical properties of Zr-based compounds

As depicted in Figs. 5 and 6, diamagnetic $\text{ZrAs}_{1.40}\text{Se}_{0.50}$ exhibits features typical of an ordinary metal [11]. The measured value of the Sommerfeld coefficient $\gamma = 1.7(\pm 0.2) \text{ mJK}^{-2}\text{mol}^{-1}$ is comparable to the electronic term in main-group metallic elements such as, e.g., In, Sn or Hg. In addition, the small residual resistivity ratio $\rho_{300\text{ K}}/\rho_0 = 1.15$ (with $\rho_0 = 140 \text{ } \mu\Omega\text{cm}$ being the residual resistivity) resembles rather dirty than pure metals and indicates a significant structural disorder in the $\text{ZrAs}_{1.40}\text{Se}_{0.50}$ crystals. This agrees well with the results of both the electron-probe microanalysis and the X-ray diffraction studies. In fact, since any deviation from the 1:1:1 stoichiometry of the system crystallizing in the PbFCl type structure always results in structural disorder. Hence, the number of imperfections is necessarily large in specimens with the chemical composition of 1:1.4:0.5.

A minimum in the resistivity at $\approx 12 \text{ K}$ is the most intriguing physical property of $\text{ZrAs}_{1.40}\text{Se}_{0.50}$. Especially the fact that virtually the same $\Delta\rho/\rho_{2\text{ K}}$ data obtained at both $B = 0$ and 9 T makes a magnetic Kondo effect most unlikely. As mentioned before, such a field-independent amplitude of the low- T upturn cannot be attributed to weak localization and/or interaction between electrons of

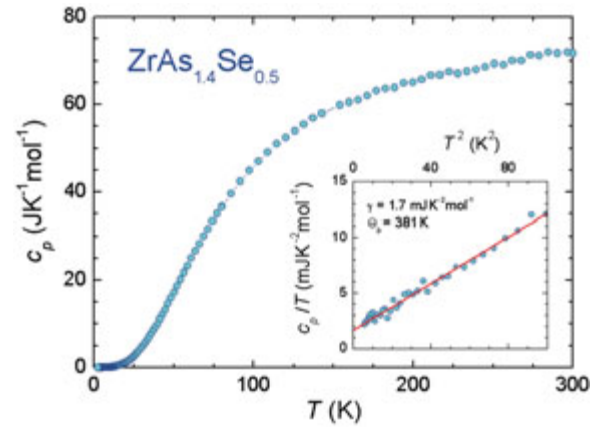


Fig. 5: Temperature dependence of the specific heat of a single crystal of $\text{ZrAs}_{1.4}\text{Se}_{0.5}$. Inset: Low-temperature specific heat, as c_p/T vs T^2 (fit shows $\gamma T + \beta T^3$, yielding $\gamma = 1.7 \text{ mJK}^{-2}\text{mol}^{-1}$ and $\Theta_D = 381 \text{ K}$).

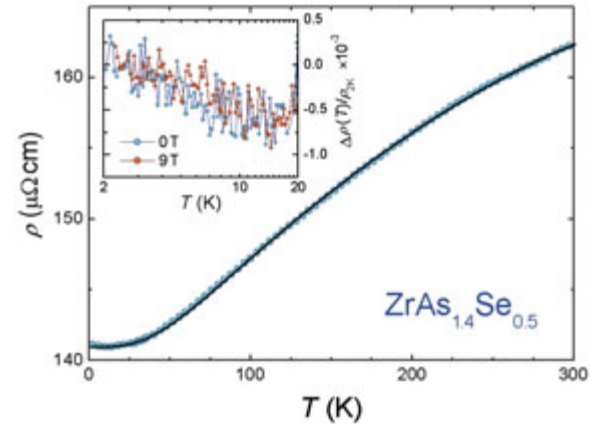


Fig. 6: Electrical resistivity as a function of temperature for a single crystal of $\text{ZrAs}_{1.4}\text{Se}_{0.5}$ (the same as that the one used for the c_p measurements shown in Fig. 5). Solid line is a fit to a generalized Bloch-Grüneisen-Mott relation with the power of $n = 3$ (see [9] for details). Inset: Relative change of the low- T resistivity $\Delta\rho(T)$ normalized to the corresponding value at 2 K, as obtained in both zero field and 9 T.

antiparallel momenta. Finally, electron-electron interaction in the particle-hole diffusion channel (electrons of parallel momenta) seems to be absent in $\text{ZrAs}_{1.40}\text{Se}_{0.50}$ as well. This can be inferred from the fact that no obvious difference between the zero-field and $B = 9 \text{ T}$ data was found at the lowest temperatures measured, where, for $g\mu_B H > k_B T$, interactions in the diffusion channel are expected to be cut off [13,14]. Forthcoming experiments at mK temperatures and in even higher magnetic fields should clarify to which extent this type of quantum corrections may influence the charge transport in Zr-based arsenide selenides. However, independent

of the outcome of these future investigations, it is fair to say that the strikingly similar $\rho(T)$ behavior of ThAsSe and ZrAs_{1.40}Se_{0.50} strongly suggests that the charge carriers in both compounds undergo the same distinct scattering process, i.e., scattering off some tunneling centers in the As-Se substructure.

As far as the $\rho(T)$ data for the PbFCl-type arsenide selenides are concerned, properties of arsenide tellurides such as ZrAs_{1.64}Te_{0.36} and ZrAs_{0.75}Te_{1.25} should be quoted. Whereas the former compound also crystallizes in the PbFCl-type structure, the latter shows an orthorhombic crystal structure (NbPS type structure). Most importantly, however, only for the tetragonal ZrAs_{1.64}Te_{0.36} we found a low- T upturn in the resistivity. Its absence in the orthorhombic derivative ZrAs_{0.75}Te_{1.25} is very remarkable and underlines the decisive role played by the PbFCl type structure.

Summary

To summarize, we have investigated a ThAsSe single crystal whose low-temperature resistivity shows a $-AT^{1/2}$ contribution. Its origin was found to be very different from the frequently observed weak-localization phenomenon, as highlighted by the independence of the resistivity on strong magnetic fields. Furthermore, the low- T thermal properties give clear evidence for the presence of tunneling centers in the sample studied. Our experimental findings lead to the suggestion of a two-channel Kondo effect originating from the interaction between the conduction electrons and structural two-level systems. A significantly similar, magnetic field-independent upturn to low-temperature $\rho(T)$ has been observed upon cooling for the related PbFCl-type compounds ZrAs_{1.40}Se_{0.50} and ZrAs_{1.64}Te_{0.36}. The results of X-ray diffraction and electron microprobe investigations on the Zr-based arsenide selenide show that a formation of tunneling centers might be triggered by the formation of As polymers or/and the mixed occupation of the $2c$ sites by arsenic and selenium. From the size of the

characteristic Kondo scale determined for ThAsSe we speculate that the tunneling particles are electrons rather than atoms.

References

- [1] *P. Nozieres and A. Blandin*, *J. Phys. (Paris)* **41** (1980) 193.
- [2] See, for a review, *D. L. Cox and A. Zawadowski*, *Adv. Phys.* **47** (1998) 599.
- [3] *A. Zawadowski*, *Phys. Rev. Lett.* **45** (1980) 211.
- [4] *I. L. Aleiner, B. L. Altshuler, Y. M. Galperin, and T. A. Shutenko*, *Phys. Rev. Lett.* **86** (2001) 2629.
- [5] *L. Borda, A. Zawadowski, and G. Zaránd*, *Phys. Rev. B* **68** (2003) 3625.
- [6] *T. Cichorek, H. Aoki, J. Custers, P. Gegenwart, F. Steglich, Z. Henkie, E. D. Bauer, and M. B. Maple*, *Phys. Rev. B* **68** (2003) 144411.
- [7] *T. Cichorek, Z. Henkie, J. Custers, P. Gegenwart, and F. Steglich*, Max-Planck-Institute for Chemical Physics of Solids, Scientific Report 2001/2002, Dresden, January 2003.
- [8] *Z. Henkie, A. Pietraszko, A. Wojakowski, L. Kępiński, and T. Cichorek*, *J. Alloys Comp.* **317-318** (2001) 52.
- [9] *T. Cichorek, A. Sanchez, P. Gegenwart, A. Wojakowski, Z. Henkie, G. Auffermann, F. Weickert, S. Paschen, R. Kniep, F. Steglich*, *Phys. Rev. Lett.* **94** (2005) 236603.
- [10] *R. L. Withers, R. Vincent, J. Schoenes*, *J. Solid State Chem.* **177** (2004) 701.
- [11] *M. Schmidt, T. Cichorek, R. Niewa, A. Schlechte, Yu. Prots, F. Steglich, R. Kniep*, *J. Phys.: Cond. Matter* **17** (2005) 5481.
- [12] *A. Schlechte, M. Schmidt, T. Cichorek, P. Simon, Yu. Prots, Th. Doert, R. Niewa, F. Steglich, R. Kniep*, *Z. Kristallogr. Suppl.* **22** (2005) 115.
- [13] *P. A. Lee and T. V. Ramakrishnan*, *Rev. Mod. Phys.* **57** (1985) 287.
- [14] *J. M. Monsterleet, B. Capoen, and G. Biskupski*, *J. Phys.: Cond. Matter* **9** (1997) 8657.

¹ Present address: Institute of Low Temperature and Structure Research, Polish Academy of Sciences, Wrocław, Poland

² Present address: TU München, München, Germany

³ Present address: Vienna University of Technology, Vienna, Austria

⁴ Institute of Low Temperature and Structure Research, Polish Academy of Sciences, Wrocław, Poland